Quadratic Program based Control of Fully-Actuated Transfemoral Prosthesis for Flat-Ground and Up-Slope Locomotion

Huihua Zhao[1] and Aaron D. Ames[2]

Abstract— **This paper utilizes a novel optimal control strategy that combines control Lyapunov function (CLF) based model independent quadratic programs with impedance control as the feed-forward term to achieve flat-ground and up-slope walking on a fully-actuated above-knee prosthesis. CLF based quadratic programs have the ability to optimally track desired trajectories; when combined with impedance control—implemented as a feed-forward term—the end result is a controller that utilizes only local information while being robust to disturbances. This control methodology is applied to a human model, i.e., a bipedal robot with anthropomorphic parameters, "wearing" a fully-actuated transfemoral prosthesis. Traditional human-inspired control methods are applied to the human component of the model—simulating nominal human walking—while the novel control method is applied to the transfemoral prosthesis. Through simulation, walking on flat-ground and up-slope is demonstrated, with the resulting gait achieved using the novel prosthesis control yielding walking that is nearly identical to the "healthy" human model. Robustness tests indicate that the prosthesis controller can endure large uncertainties and unknown disturbances.**

I. INTRODUCTION

Impedance control has been a popular approach for the control of both prosthesis [12], [24], [25] and orthosis [16], [14] in recent decades. An ankle orthosis in [13] has been designed using PD control in the swing phase and variable impedance control in the stance phase. Impedance control for a fully-actuated knee-ankle prosthesis can be found in [24]. Combined with using EMG signals for motion intent recognition, impedance control has been successfully applied for a ankle-foot prosthesis in [11]. However, impedance control has serious problems with maintaining good tracking and robustness, which will be addressed in this work.

While implementing controllers for an amputee, there are basic biomechanical requirements that must be satisfied for a transtibial or transfemoral prosthesis [21], [26]: (1) the prosthetic device must support the body weight of the amputee during the stance phase, i.e., the prosthesis control should provide "stability" during the weight bearing phase; (2) the physical interface between the able body and the prosthesis must prevent undesirable pressure during the locomotion; (3) the prosthesis has to duplicate as nearly as possible the kinematics of the normal gait, i.e., the amputee should walk with normal appearance as if they were able bodied.

*This research is supported by NASA grant NNX11AN06H, NSF grants CNS-0953823 and CNS-1136104, and NHARP award 00512-0184-2009.

[1]HH.Zhao is with the department of Mechanical Engineering, TAMU, 3128 TAMU, College Station, USA huihuazhao@tamu.edu

[2]Prof. A.Ames is with department of Mechanical Engineering and Electrical Engineering, Texas A & M University, 3128 TAMU, College Station, USA aames@tamu.edu

The goal of this paper is to address requirements (1) and (3) indicated above on a fully-actuated above-knee prosthesis for different types of motion. This goal will be achieved with three steps. Firstly, traditional human-inspired control methods are reviewed and applied to the human component of the model to obtain intact human trajectories for both flat-ground walking and up-slope walking, based on which, the impedance parameters can be estimated. Then, impedance control is implemented on the prosthesis joints, showing that the estimated parameters are robust enough to work on the prosthesis. Finally, a novel prosthesis control method: control Lyapunov function based quadratic programs (QPs) coupled with impedance control has been applied to the prosthesis. The end results indicate improved tracking performance and robustness to unknown disturbances.

Based loosely on the definition of impedance control first proposed by Hogan [15], the torque at each joint during a single step cycle can be represented by a series of passive impedance functions [24]. By reproducing this torque at the prosthetic device joint using the passive impedance functions, one can obtain similar prosthetic gaits compared to those found in normal gait tests. Normally, hand tuning from an expert is required to obtain the impedance parameters [10], [19]; therefore, this leads to another disadvantage—it is not optimal, i.e., when the prosthesis is off the desired trajectory, it may generate large torque while driving the device back to the equilibrium point. By only using impedance control, we are able to achieve stable robot walking with prosthetic device (the stabilities are numerically verified with using Poincarè map). However, considering all the drawbacks of impedance control, the obtained tracking performance is lacking, resulting in walking that is not as robust as desired.

Utilizing the impedance controller as a feed-forward term, we present a novel control method that will be utilized as a feedback term to increase robustness and stability. In particular, we begin by considering rapidly exponentially stabilizing control Lyapunov functions (RES-CLFs) as introduced in [8]. This class of CLFs can naturally be stated as inequality constraints in torque such that, when satisfied, rapid exponential convergence of the error is formally guaranteed. Furthermore, these inequality constraints can naturally be solved in an optimal fashion through the use of quadratic programs. The end result is a CLF based QP. Finally, due to the special structure of the RES-CLFs that will be considered in this paper, the CLF based QP can be stated in a model independent fashion. The end result is a novel feedback control methodology: Model Independent Quadratic Programs (MIQP) based upon RES-CLFs. These

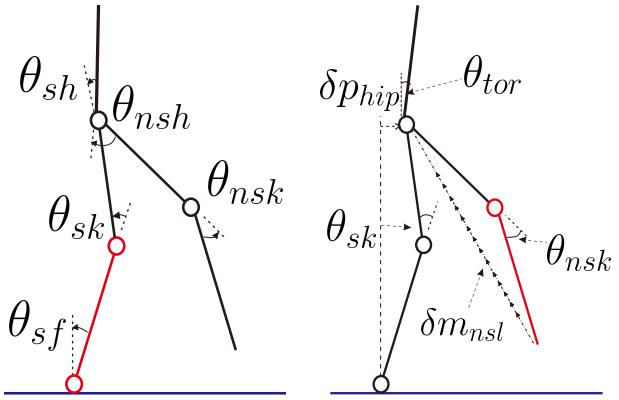

Fig. 1: The angle conventions with prosthetic leg as stance leg (left) and the outputs description with prosthetic leg as swing leg (right). The red line denotes the prosthetic device; the red circle represents the prosthesis joint that will be controlled using prosthetic controller.

are combined with impedance control to obtain the final prosthetic controller. With the proposed controller, we will show that the tracking performance can be improved in simulation for both types of locomotion. In addition, utilizing this novel control method, the robot displays improved stability and robustness to unknown disturbances.

This paper begins with an introduction of the mathematical modeling of a hybrid system in Sec. II; a brief review of human-inspired optimization is also covered for obtaining human-like walking gaits. Controller construction of the impedance control is discussed in Sec. III. Simulation results are presented at the end of this section. Then the CLF model independent control will be discussed in detail in Sec. IV. Simulation results by using this controller are discussed and compared with using only an impedance controller. Finally, the discussion and future work will be discussed in Sec. V.

II. Human-Inspired Optimization

In this section, the mathematical modeling of a hybrid robot model is covered, and the traditional human-inspired control method is introduced to apply to the human component of the model [6]. Finally, human-inspired optimization [22] is discussed to obtain human-like flat-ground and up-slope locomotion.

A. Robot Model

A planar bipedal robot that has five serial chain links (one torso, two thighs and two calves) with anthropomorphic parameters, has been considered as the human model. As bipedal robotic walking displays both continuous and discrete behavior (when foot impacts the ground), we formally represent the bipedal robot as a hybrid system (see [6] for the formal definition). The explanations will be discussed in the following sections explicitly.

Continuous Dynamics. The configuration space of the robot Q_R is described in body coordinates as: $\theta = (\theta_{sf}, \theta_{sk}, \theta_{sh}, \theta_{nsh}, \theta_{nsk})^T$, the angle definitions are shown in Fig. 1. Since we are considering human walking with transfemoral prosthesis, the mass and length properties corresponding to the average human model [6] are utilized to derive the equations of motion of the robot, which are given using the Euler-Lagrange formula:

$$D(\theta)\ddot{\theta} + H(\theta, \dot{\theta}) = Bu, \tag{1}$$

where $D(\theta)$ is the inertial matrix and torque map $B = I_5$ (considering the robot is fully-actuated), and the control, u, is the vector of torque inputs. Manipulation of (1) yields the affine system (f, g) for the continuous dynamics [6].

Discrete Dynamics. When the swing foot hits the ground, a discrete impact will happen, which leads to the velocity changes of the robot, combining with a leg switch simultaneously. With the perfect plastic impact assumptions, the method of [17] is used to get the reset map Δ_R as:

$$\Delta_R(\theta, \dot{\theta}) = \begin{bmatrix} \Delta_\theta\, \theta \\ \Delta_{\dot{\theta}}(\theta)\, \dot{\theta} \end{bmatrix}, \tag{2}$$

where Δ_θ is the relabeling matrix which switches the stance and non-stance leg at impact, and $\Delta_{\dot{\theta}}$ determines the change in velocities due to the impact [6].

B. Human-Inspired Optimization

With the model discussed above, human-inspired optimization will be reviewed to obtain the motion primitives, which are flat-ground and up-slope walking in this work.

Human Outputs. With the goal to achieve human-like bipedal robotic walking, a human-inspired controller aims to drive the actual robot outputs $y_a(\theta)$ [1] , to the desired human outputs $y_d(t, \alpha)$ which can be represented by the CWF introduced in [6]. Therefore, we are motivated to introduce the human-inspired outputs:

$$y(\theta, \dot{\theta}) = \begin{bmatrix} y_1(\theta, \dot{\theta}) \\ y_2(\theta) \end{bmatrix} = \begin{bmatrix} y_1^a(\theta, \dot{\theta}) - v_{hip} \\ y_2^a(\theta) - y_2^d(\tau(\theta), \alpha) \end{bmatrix}, \tag{3}$$

where $y_1(\theta, \dot{\theta})$ is the relative degree one output, which is the difference between the actual forward hip velocity $y_1^a(\theta, \dot{\theta})$ and the desired hip velocity v_{hip}. And $y_2(\theta)$ are the relative degree two human-inspired outputs which are the difference between the actual relative degree two outputs $y_2^a(\theta)$ and desired relative degree two outputs $y_2^d(\tau(\theta), \alpha)$, defined as:

$$y_2^a(q) = \begin{bmatrix} \theta_{sk} \\ \theta_{nsk} \\ \delta m_{nsl}(\theta) \\ \theta_{tor}(\theta) \end{bmatrix}, \; y_2^d(\tau(\theta), \alpha) = \begin{bmatrix} y_H(\tau(\theta), \alpha_{sk}) \\ y_H(\tau(\theta), \alpha_{nsk}) \\ y_H(\tau(\theta), \alpha_{nsl}) \\ y_H(\tau(\theta), \alpha_{tor}) \end{bmatrix}, \tag{4}$$

where $\tau(\theta)$ is the parameterized time aiming to remove the time dependency of human-inspired control (the detail explanation is discussed in [6]). By grouping the parameters, we are able to form the control parameters $\alpha = (v_{hip}, \alpha_{sk}, \alpha_{nsk}, \alpha_{nsl}, \alpha_{tor}) \in \mathbb{R}^{21}$.

[1]The outputs considered in this work are linearized hip position δp_{hip}, linearized non-stance slope δm_{nsl}, two knee angles $\theta_{sk}, \theta_{nsk}$ and the torso angle θ_{tor} (as denoted in Fig. 1).

With this construction in hand, we represent the dynamics (1) in outputs space by differentiating the $y(\theta,\dot{\theta})$ twice:

$$\begin{bmatrix}\dot{y}_1\\ \ddot{y}_2\end{bmatrix} = \underbrace{\begin{bmatrix}L_f y_1(\theta,\dot{\theta})\\ L_f^2 y_2(\theta,\dot{\theta})\end{bmatrix}}_{L_f} + \underbrace{\begin{bmatrix}L_g y_1(\theta,\dot{\theta})\\ L_g L_f y_2(\theta,\dot{\theta})\end{bmatrix}}_{A} u, \tag{5}$$

where L_f is the *Lie* derivative and A is the dynamic decoupling matrix, which is nonlinear in most cases. By picking:

$$u = A^{-1}(L_f + \mu), \tag{6}$$

with μ properly designed as:

$$\mu = \begin{bmatrix}L_f y_1(\theta,\dot{\theta})\\ 2\xi L_f y_2(\theta,\dot{\theta})\end{bmatrix} + \begin{bmatrix}2\xi y_1(\theta,\dot{\theta})\\ \xi^2 y_2(\theta)\end{bmatrix}, \tag{7}$$

one can drive both $y_1 \to 0$ and $y_2 \to 0$ in a provably exponentially stable fashion, which we term the human-inspired controller. ξ is the controller gain that determines the convergence rate, details of which are referred to in [6].

Partial Hybrid Zero Dynamics. In particular, we are focusing on relative degree 2 outputs, $y_2 = y_2^a - y_2^d$, while relaxing relative degree 1 output to compensate for the model difference between the robot and human (see [6] for detailed discussion). The surface for which these outputs agree for all time is given by the *partial zero dynamics surface*:

$$\mathbf{PZ}_\alpha = \{(q,\dot{q}) \in T\mathscr{Q} : y_2(q) = \mathbf{0},\ L_f y_2(q,\dot{q}) = \mathbf{0}\}. \tag{8}$$

While the proposed controller (6) renders exponential convergence to this surface, the robot will be "thrown-off" the surface when impact happens. The goal of *partial hybrid zero dynamics* (PHZD) is to find parameters α that ensure that this surface remains invariant through impacts: $\Delta(S \cap \mathbf{PZ}_\alpha) \subset \mathbf{PZ}_\alpha$. This constraint motivates the introduction of an optimization problem that guarantees this condition.

Human-Inspired Optimization. Aiming to find the parameters α yields provable stable human-like robotic walking, an optimization problem subject to PHZD constraints is given:

$$\alpha^* = \underset{\alpha\in\mathbb{R}^{21}}{\operatorname{argmin}}\ \mathrm{Cost}_{\mathrm{HD}}(\alpha) \tag{HIO}$$

$$\text{s.t} \quad \textit{PHZD} \tag{C1}$$

where, the cost function (HIO) is the least-square-fit errors between human experimental data and the CWF representations [6]. Note that, including the PHZD constraints which guarantee exponentially stable orbits in hybrid systems (see [6] for formal proof), auxiliary constraints, such as foot scuffing prevention and maximum knee angles, are also imposed to help generate walking gaits that are as human-like as possible.

Solving the optimization problem discussed above, we can obtain the parameters for both flat-ground walking α_l and up-slope walking α_r, which we term *motion primitives* (see [22] for more discussions). The gait tiles for both motion primitives using the human-inspired controller are shown in Fig. 2 and the limit cycles can be seen in Fig. 3. In particular, these results are going to be used as the nominal references of "unimpaired" human walking. This

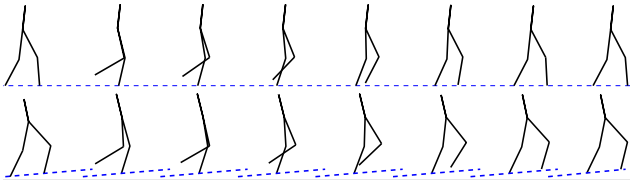

Fig. 2: Gait tiles using human-inspired controller for flat-ground walking and up-slope walking.

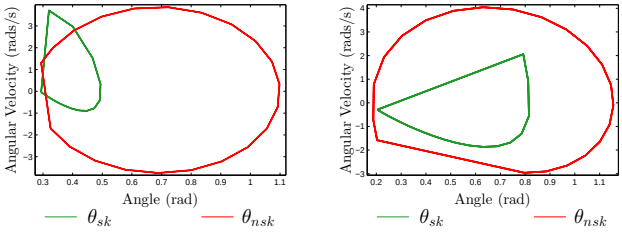

(a) Flat-ground walking (b) Up-slope walking

Fig. 3: Phase portraits of the walking gaits using human-inspired control.

controller utilizes complete knowledge about the bipedal system to replicate human trajectories, which, however, is not available to the prosthetic device. Therefore, a prosthesis controller that only requires "local" information—joint angle and angular velocities of the prosthetic device—is motivated to be introduced in the following sections.

III. IMPEDANCE CONTROL CONSTRUCTION

In this section, the general idea of impedance control will be introduced first. Impedance parameter estimation algorithm will be discussed to obtain the impedance parameters automatically for different motion primitives. Finally, simulation results of using impedance control will be presented.

A. Impedance Control for Prosthesis

Impedance Control. Based on the notion of impedance control first proposed by Hogan [15], the torque at each joint during a single step can be piecewisely represented by a series of passive impedance functions [24] with the form:

$$\tau = k(\theta - q^e) + b\dot{\theta}, \tag{9}$$

where impedance parameters k, q^e and b represent the stiffness, equilibrium point and damping respectively, and are constant during specific sub-phase of particular motion primitive. This formula only requires local information—in this case, the right knee angle and foot angle—therefore, the end result is a simple prosthesis control.

Phase Separation. With the assumption that human gait is cyclical, impedance control with a finite state machine is one of the most used algorithms suggested to date [18]. One main problem is to identify the sub-phases correctly of one single step cycle of different motion primitives, which will be discussed in this section.

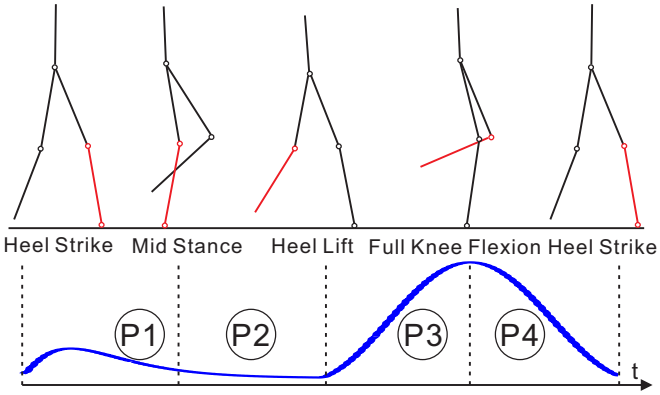

Fig. 4: AMBER gait phase separation. The red line represents the prosthetic device and the red circles are the actuated prosthesis joints. The black lines denote the able body and black cirlces indicate the actuated healthy joints. The green line is the knee angle of one full gait cycle.

Based on the previous work of flat ground walking [5], analysis of data obtained from human model shows that one gait cycle can be divided into four phases based on the profile of prosthesis joint angles, which are denoted as $p = 1,2,3,4$, as shown in Fig. 4. Specifically, each phase begins at time t_0^p and ends at t_f^p. The phase separation principle is similar to that in [5] but with different values specific to different motion types, which can be referred to Table I. The impedance torque at the prosthesis joints (right knee joint and right foot joint) during a phase $p \in \{1,2,3,4\}$, can be represented by the following equation:

$$\tau_p^{imp} = k_p(\theta_{ps}(t) - q_p^e) + b_p\dot{\theta}_{ps}(t), \tag{10}$$

where $\theta_{ps}(t)$ and $\dot{\theta}_{ps}(t)$ denote angles and angular velocities of the prosthesis joints at time t. In particular, we have $\theta_{ps} = \{\theta_{sf}, \theta_{sk}\}$ when the prosthesis leg is the stance leg; and $\theta_{ps} = \theta_{nsk}$ when the prosthesis leg is in the swing phase. Therefore, in each phase p, the dynamics of the biped system are governed by the following Euler-Lagrange equations:

$$\begin{cases} D(\theta)\ddot{\theta} + H(\theta,\dot{\theta}) = Bu & \forall t \in [t_0^p, t_f^p], \\ (\theta(t_0^p), \dot{\theta}(t_0^p)) = R(\theta(t_f^{p-1}), \dot{\theta}(t_f^{p-1})), \end{cases} \tag{11}$$

where $p-1 = 4$ if $p = 1$ and the switching function R has been defined as the following:

$$R(\theta(t),\dot{\theta}(t)) = \begin{cases} \Delta(\theta(t),\dot{\theta}(t)) & \textit{at} \text{ impacts} \\ (\theta(t),\dot{\theta}(t)) & \text{otherwise.} \end{cases} \tag{12}$$

Specifically, for the prosthesis joints, we will replace the corresponding u_i term with the prosthetic control input τ_p^{imp}, which yields the following set up:

$$D_i(\theta)\ddot{\theta} + H_i(\theta,\dot{\theta}) = \tau_p^{imp} \qquad \forall t \in [t_0^p, t_f^p], \tag{13}$$

where i indicates the ith row of the corresponding term in (11), which will be updated according to the sub-phase p. Note that, since we define the body coordinates based on the stance and non-stance nomenclature, we have $i = 1,2$ if $p = 1,2$, i.e., the prosthetic device is the non-stance leg, and $i = 5$ if $p = 3,4$, i.e., the prosthetic device is the swing leg.

TABLE I: Estimated Impedance Parameters of the Prosthesis Knee Joint.

Motion Type	Phase	Phase Separation	k_p[Nm]	b_p[Nms]	q_b^e[rad]
Flat-ground	**P1**	heel strike	-574.97	-133.54	0.9867
	P2	$\theta_{sf} < -0.01$	-642.23	8.6826	0.3297
	P3	heel lift	-5.7679	0.3378	1.0042
	P4	$\dot{\theta}_{nsk} < 0$	-16.186	0.5472	1.1402
Up-slope	**P1**	heel strike	-338.44	-4.4349	0.2878
	P2	$\theta_{sf} < -0.25$	-216.38	17.859	0.2024
	P3	heel lift	-6	-0.9626	1.1342
	P4	$\dot{\theta}_{nsk} < 0$	-25.944	-0.0634	1.2473

Impedance Parameter Estimation. With the phase transitions defined above, the next goal is to identify the impedance parameters for each phase of different motion primitives.

In the previous work [5], the authors showed that the impedance parameters of the knee joint for a lower-limb prosthesis can be learned by the observation of unimpaired human walking data, which is realized by the human-inspired control in simulation. The results have been validated in both simulation and experiment with a transfemoral prosthetic device (video with more details can be seen in [2]). To extend these results, we utilize a similar method to estimate the impedance parameters of multiple joints by observing the simulated "unimpaired" motion primitive data.

We first obtain the "unimpaired" walking data (which are the joint angles and velocities $x = (\theta_{ps}, \dot{\theta}_{ps})$ and joint torques τ_{ps}) by using the human-inspired controller. By defining the impedance parameter set as $\beta_p = \{k_p, b_p, q_p^e\}$ for specific sub-phase p, we can form the least square errors minimization problem as follows:

$$\beta_p^* = \underset{\beta_p}{\text{argmin}} \int_{t_0^p}^{t_f^p} (\tau_p^{imp} - \tau_{ps,p})^2 dt, \tag{14}$$

where τ_p^{imp} is defined as (10) and $\tau_{ps,p}$ is the "healthy" input torque on the prosthesis joints at sub-phase p. By solving this minimization problem, the estimated impedance parameters for each sub-phase can be seen in Table. I. Note that, we only show the parameters for the knee joint since the prosthesis ankle joint is only actuated at phase p_1 and p_2. The parameters of the ankle joint can be sent on request.

B. Simulation Results

With the obtained impedance parameters, the walking of an amputee "wearing" a tranfemoral prosthesis with an actuated ankle and knee is simulated using only impedance control. The gait tiles in Fig. 5 indicate that good walking has been achieved for both modes of locomotion. The phase portraits for 32 steps of both motion primitives are also shown in Fig. 6a, 6b. The Poincarè map has been utilized to numerically prove that both motion primitives (with prosthesis joints controlled using impedance controller) are stable with the max eigenvalues less than a unit (the maximum eigenvalue is 0.34) [20]. Tracking results along with *RMS*

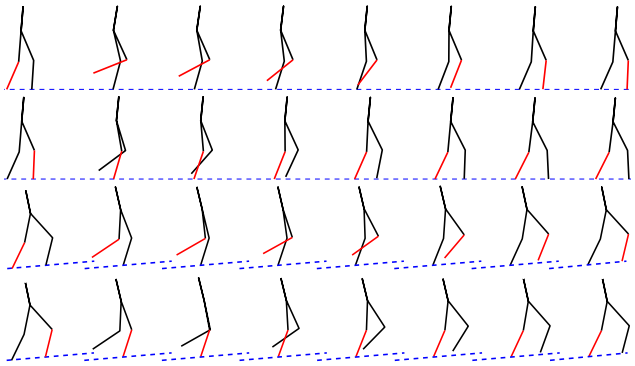

Fig. 5: Gait tiles using impedance control for level walking and slope walking. Red line indicates the prosthesis.

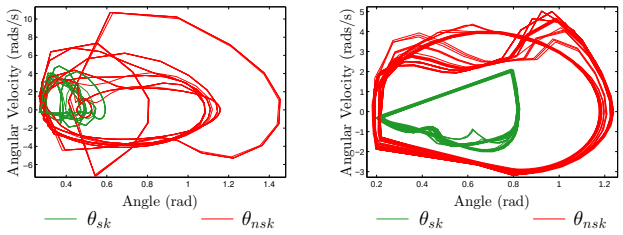

(a) Flat-ground walking phase portrait (b) Up-slope walking phase portrait

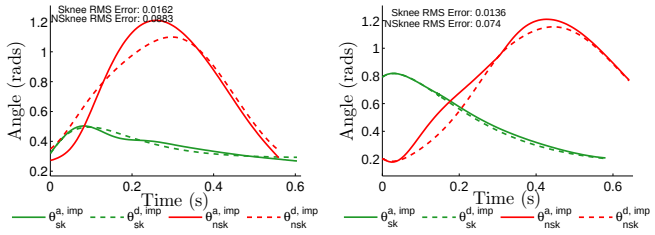

(c) Flat-ground prosthesis knee outputs (d) Up-slope prosthesis knee outputs

Fig. 6: Phase portraits and outputs of the prosthesis knee joint with using only impedance control.

errors are presented in Fig. 6c, 6d. Detailed discussions about the performance comparisons between using the impedance controller and using the novel controller will be covered later.

IV. MIQP + Impedance Control

In this section, we will start with the introduction of rapidly exponentially stabilizing control Lyapunov functions (RES-CLFs) first introduced in [8]. The quadratic programs method is utilized to realize the CLF, when combined with the impedance control (implemented as a feed-forward term), the end result is a novel model independent feedback control methodology: Model Independent Quadratic Programs (MIQP) + Impedance control. The simulation results showing better tracking performance, improved stability and robustness, are discussed at the end.

A. CLF MIQP

As discussed in Sec. II, by designing μ properly, [6] for example, exponential convergence tracking can be achieved using the human-inspired controller. This control strategy works well for nonlinear systems [23] if we have a good knowledge about the model; however, this is usually not satisfied. PID control still dominants in the real world control problems since it does not require accurate model information, i.e., it is model independent. However, considering all the well-known problems of PID control (hand tuning, none optimal [9]), we are motivated to find a new optimal control strategy to overcome these issues while maintaining the model insensitive property.

We begin with substituting the control input (6) to equation (5), yielding the output dynamics to a linear form:

$$\begin{bmatrix} \dot{y}_1 \\ \ddot{y}_2 \end{bmatrix} = \mu. \tag{15}$$

With defining the vector $\eta = (y, \dot{y}) \in \mathbb{R}^{2\times(n_1+n_2)}$ with n_1, n_2 denoting the numbers of relative degree one outputs and relative degree two outputs correspondingly, equation (15) can be written as a linear affine control system:

$$\dot{\eta} = \underbrace{\begin{bmatrix} 0_{n_1+n_2} & I_{n_1+n_2} \\ 0_{n_1+n_2} & 0_{n_1+n_2} \end{bmatrix}}_{F} \eta + \underbrace{\begin{bmatrix} 0_{n_1+n_2} \\ I_{n_1+n_2} \end{bmatrix}}_{G} \mu. \tag{16}$$

In the context of this control system, we consider the Continuous Algebraic Riccati Equations (CARE):

$$F^T P + PF - PGG^T P + I = 0, \tag{17}$$

where $P = P^T > 0$. With the optimal solution $\mu = -G^T P\eta$, we obtain the optimal control law that minimizes the cost:

$$\int_0^\infty (\eta^T \eta + \mu^T \mu) dt. \tag{18}$$

With the aim to have stronger bounds of the convergence of the considered hybrid system with impacts, we take this method further by defining $\eta_\varepsilon = (y/\varepsilon, \dot{y})$ in order to obtain exponentially stable orbit. Then, we can choose P and $\varepsilon > 0$ carefully to construct a *rapid exponentially stabilizing control Lyapunov function (RES-CLF)* that can be used to stabilize the output dynamics with a rapid exponentially fashion (the proof with details can be seen in [9]). In particular, we define the positive definite CLF as:

$$V_\varepsilon(\eta) = \eta^T \begin{bmatrix} \frac{1}{\varepsilon} I & 0 \\ 0 & I \end{bmatrix} P \begin{bmatrix} \frac{1}{\varepsilon} I & 0 \\ 0 & I \end{bmatrix} \eta := \eta^T P_\varepsilon \eta. \tag{19}$$

Differentiating this function renders:

$$\dot{V}_\varepsilon(\eta) = L_f V_\varepsilon(\eta) + L_g V_\varepsilon(\eta)\mu, \tag{20}$$

where $L_f V_\varepsilon(\eta) = \eta^T (F^T P_\varepsilon + P_\varepsilon F)\eta$, $L_g V_\varepsilon(\eta) = 2\eta^T P_\varepsilon G$.

In order to exponentially stabilize the system, we want to find μ such that, for specifically chosen $\gamma > 0$ [9], we have:

$$L_f V_\varepsilon(\eta) + L_g V_\varepsilon(\eta)\mu \leq -\frac{\gamma}{\varepsilon} V_\varepsilon(\eta). \tag{21}$$

Therefore, an optimal μ could be found by solving the following quadratic program (QP) as:

$$m(\eta) = \underset{\mu\in\mathbb{R}^{n_1+n_2}}{\operatorname{argmin}} \ \mu^T \mu \tag{22}$$

$$\text{s.t} \quad \varphi_0(\eta) + \varphi_1(\eta)\mu \leq 0, \tag{CLF}$$

TABLE II: RMS Errors with Using Different Controllers.

Motion	**Flat-ground**		**Up-slope**	
Joints	Impedance	MIQP+Impedance	Impedance	MIQP+Impedance
θ_{sf}	0.0181	0.0053	0.0174	0.0033
θ_{sk}	0.0162	0.0017	0.0136	0.0007
θ_{nsk}	0.0883	0.0009	0.074	0.0045

where $\varphi_0(\eta) = L_f V_\varepsilon(\eta) + \frac{\gamma}{\varepsilon} V_\varepsilon(\eta)$ and $\varphi_1(\eta) = L_g V_\varepsilon(\eta)$.

Note that, instead of substituting the optimal solution μ into equation (6) to obtain the feedback control law as in [7], we use μ directly as control input into the original system without considering the model decoupling matrix A and L_f. Therefore, we term this strategy *Model Independent Quadratic Program* (MIQP) controller.

Taking a further look into the MIQP algorithm, we basically constructed a new linear control system (16) that only focuses on the errors between the actual outputs and desired outputs, while not requiring any information about the original model. Another immediate advantage is that torque bounds can be directly applied in this formulation; thus, the optimal control value can be obtained while respecting the torque bounds. As discussed in [7], this can be achieved by relaxing the CLF constraints with a large penalty value $p > 0$. In particular, we consider the MIQP as:

$$\begin{aligned} \underset{(\delta,\mu)\in\mathbb{R}^{n_1+n_2+1}}{\text{argmin}} \quad & p\delta^2 + \mu^T\mu && (23)\\ \text{s.t} \quad & \varphi_0(\eta) + \varphi_1(\eta)\mu \le \delta, && \text{(CLF)}\\ & \mu \le \mu_{MAX}, && \text{(Max Torque)}\\ & -\mu \le \mu_{MAX}. && \text{(Min Torque)} \end{aligned}$$

Similarly, for the control of human model, the term μ can be replaced with the input torque τ^{qp} directly. By solving this QP problem, an optimal controller can be obtained to regulate the output dynamics with a rapid exponentially stable fashion for the hybrid bipedal system.

B. MIQP + Impedance Control

Utilizing the formal work discussed above, we are now ready to introduce the novel CLF based control algorithm of this paper, which is the MIQP + Impedance control algorithm for prosthesis control.

While MIQP control benefits its model independent property and optimal fashion in practical application, it also suffers the over shooting problem as the PID controller does considering its lacking of model information. Particularly, over shooting issue will be a fatal problem for the prosthesis controller with the safety consideration of an amputee, therefore, motivates the proposal of MIQP + Impedance control.

With considering the impedance control τ^{imp} as the feed-forward term, the input torque u_{ps} of the prosthesis joint, or the system (16) can be stated as the following:

$$u_{ps} = \tau^{qp} + \tau^{imp}, \tag{24}$$

where τ^{qp} is the torque computed from the MIQP problem. To take a further step, we add the impedance term τ^{imp} into the MIQP construction, which yields the following MIQP + Impedance problem:

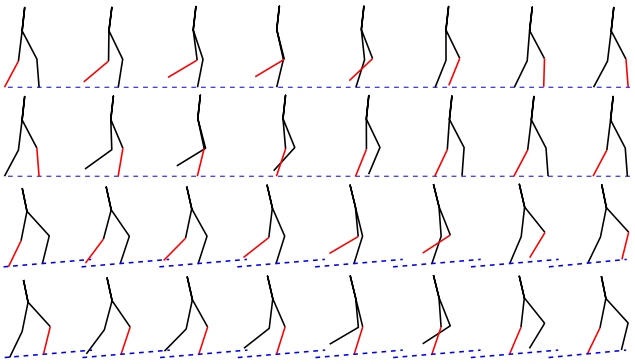

Fig. 7: Gait tiles using MIQP + Impedance control for level walking and slope walking. Red line indicates the prosthesis.

$$\begin{aligned} \underset{(\delta,\tau^{qp})\in\mathbb{R}^{n_1+n_2+1}}{\text{argmin}} \quad & p\delta^2 + \tau^{qpT}\tau^{qp} && (25)\\ \text{s.t} \quad & \varphi_0(\eta) + \varphi_1(\eta)\tau^{qp} \le \delta, && \text{(CLF)}\\ & \tau^{qp} \le \tau^{qp}_{MAX}, && \text{(Max QP Torque)}\\ & -\tau^{qp} \le \tau^{qp}_{MAX}, && \text{(Min QP Torque)}\\ & \tau^{qp} \le \tau_{MAX} - \tau^{imp}, && \text{(Max Input Torque)}\\ & -\tau^{qp} \le \tau_{MAX} + \tau^{imp}. && \text{(Min Input Torque)} \end{aligned}$$

By adding the impedance control as feed-forward term into the input torque, the model independent output dynamics system (16) gathers some information about the system that it is controlling, therefore can adjust the τ^{qp} accordingly to accommodate the feed-forward term in order to achieve perfect tracking. By setting the QP torque bounds τ^{qp}_{MAX}, we can control the overshooting problem. Note that, we also set the total input torque bounds for the QP problem such that the final optimal input torque (24) will satisfy the total torque bounds, which is critical for practical implementation.

To summarize, with the combination of the advantages from both the impedance controller which is derived from the model and the MQIP controller that is optimal for tracking, the MIQP + Impedance control method generates a better tracking performance due to the optimal nature of the controller, while rendering better uncertainty tolerance and disturbance rejection properties simultaneously. In the preceding sections, this controller will be implemented in both flat-ground walking and up-slope walking.

C. Simulation Results

Considering the different numbers of actuatation applied in swing phase and stance phase, the MIQP + Impedance controller has to be constructed accordingly. In particular, during the phase in which the prosthetic device is the stance leg, both knee and ankle are actuated; therefore, the outputs we choose are the linearized hip position δp_{hip} and stance knee angle θ_{sk}, i.e., we have $n_1 = 1$ and $n_2 = 1$. For the phase in which the prosthetic device is the swing leg, only the prosthesis knee joint is actuated; thus, the output θ_{nsk} is chosen, i.e., $n_1 = 0$ and $n_2 = 1$.

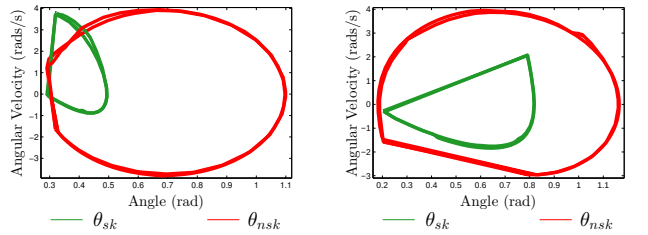

(a) Flat-ground walking phase portrait (b) Up-slope walking phase portrait

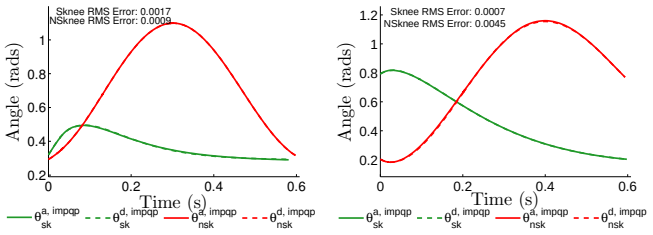

(c) Flat-ground prosthesis knee outputs (d) Up-slope prosthesis knee outputs

Fig. 8: Phase portraits and outputs of the prosthesis knee joint with MIQP + Impedance control.

With the control architecture in hand, the simulation results will be discussed in this section. The results of using different controllers (only impedance control and MIQP + Impedance control) are compared and discussed. Note that, with the exception of the prosthesis joints, on which we will use the proposed prosthesis controllers, the remaining joints will be actuated with the human-inspired control discussed in Sec. II-B.

Tracking Performance. The gait tiles of both flat-ground walking and up-slope walking are shown in Fig. 7. The tracking results of the prosthesis knee joint for both motion primitives are shown in Fig. 8a and 8b and the tracking *RMS* errors are all less than 0.005rad, which is at least 3 times better than just using impedance control. Beside that, the tracking on the ankle angle is also near perfect and the *RMS* error for the ankle tracking is less than 0.005rad. The more explicit tracking errors of all the prosthesis joints with using different controllers are shown in Table II. The phase portraits for 32 steps of both motion primitives can be seen in Fig. 8. Note that, compared to the phase portraits using human-inspired controller as shown in Fig. 3, even though we have two asymmetric controllers on two knee joints—human-inspired controller for "healthy" knee joint and MIQP + Impedance controller for "prosthesis" knee joint—the phase portraits almost converge to one limit cycle quickly. That is to say, with the proposed controller, the prosthesis can duplicate the kinematics of the normal gait; therefore, the amputee can achieve walking gaits that are nearly identical to unimpaired human walking.

Robustness Tests. Stability is another critical requirement for a lower-limb prosthesis controller. The prosthetic device must be robust and stable enough to endure unknown environment disturbances. In simulation, we show that the

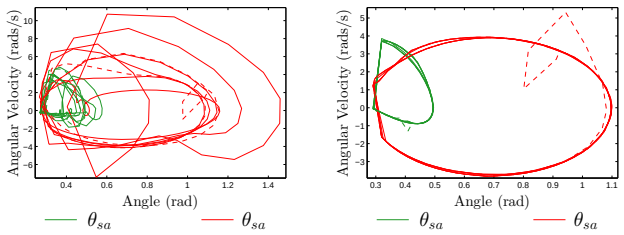

(a) Impedance Control. (b) MIQP + Impednce Control.

Fig. 9: Phase portrait of 8N impulse disturbance rejection. The dash lines represent the disturbances.

proposed MIQP + Impedance controller renders more robustness to the prosthetic device than only using impedance control, therefore, is safer for the amputees' daily use. In this section, two robustness tests have been applied to the human robot model wearing a fully-actuated prosthesis device; one is to add an instantaneous push to the prosthesis leg and another one is to let the robot walk above an obstacle.

1) Reaction to impulse push: Impulse forces (lasting for 0.01s) with different values have been applied to the prosthetic leg for both swing phase and stance phase. The maximum impulse force that the robot can tolerate and maintain good tracking with the proposed MIQP + Impedance controller is 30N. We also tested the similar impulse disturbance with only using impedance control, however, the maximum impulse force that the robot can endure is 10N; moreover, the tracking will become worse after the disturbance and, as a result, leads to a failure of walk eventually.

In order to compare the disturbance rejection properties of these two controllers more explicitly, we apply the same impulse force (6N) on the prosthesis knee joint that controlled with different controllers. The phase portraits for 8 steps of using these two controllers are shown in Fig. 9, from which,

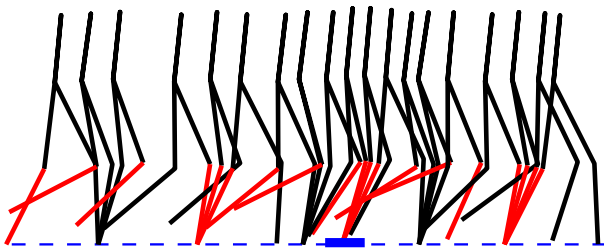

(a) Impedance Control.

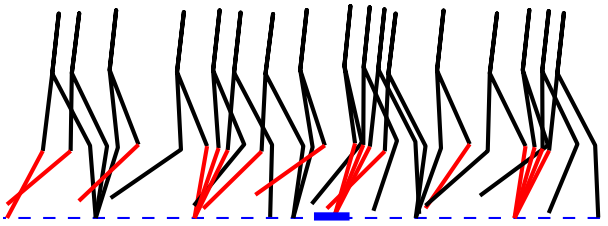

(b) MIQP + Impednce Control.

Fig. 10: Gait tiles of walking over a 20mm obstacle.

we can see that the phase portrait of MIQP + Impedance control can converge back to the limit cycle quickly and stably without generating large spikes. However, the phase portrait of using only impedance control has large velocity spikes and can not converge to the original track. A video [4] has been attached to show the details.

2) To overcome an obstacle: In the simulation, we let the robot walk over a 20mm obstacle on flat ground. The gait tiles can be seen in Fig. 10b, which shows that the robot can overcome the obstacle smoothly and keep walking as normal with using the MIQP + Impedance control. A similar test is also conducted with only using the impedance control, gait tiles of which can be seen in Fig. 10a. The robot can also walk over the obstacle, however, the tracking performance of using only impedance is worse, the details of which can be seen in the video [4].

V. CONCLUSIONS AND FUTURE WORK

Utilizing the human model with anthropomorphic parameters, "wearing" a fully-actuated above-knee prosthesis, we successfully implemented a novel optimal control strategy on this testbed to achieve flat-ground and up-slope locomotion. The proposed MIQP + Impedance controller benefits both the feed-forward impedance control that gives us model information and the MIQP method that renders model independence in an optimal fashion that is inherited from the CLF based QP control method. This method has already been applied to a physical robot AMBER with only the knee joint actuated. The experimental results showed improved tracking performance (more than 50% improvement w.r.t *RMS* error), stability, and robustness to unknown disturbances (more details can be seen in video [1]).

Extended from these results, two main contributions are presented in this work. First, we successfully implemented the proposed controller on both knee and ankle joints. By only using impedance controller with the estimated parameters, we could achieve stable walking for both motion primitives. However, due to the drawbacks of impedance control, these walking are not robust and can not reject big disturbances especially for a fully actuated prosthesis. Thus, we implemented the proposed MIQP + Impedance control; the end result is a more robust and stable prosthetic control that can replicate nearly perfect healthy human trajectories. Another contribution of this paper is that we were able to achieve up-slope walking with both impedance control and MIQP + Impedance control. Similarly, the MIQP + Impedance control renders improved tracking and robustness.

Future Work. In this work, only a point foot model is considered, which limits the ability to capture the whole picture of human locomotion. A more sophisticated model with heel lift and toe strike will be considered to test the proposed MIQP + Impedance controller in the following research. In the future work, this controller will be tested on a footed robot AMBER2, which has achieved good human-like walking with both knee and ankle actuated, the video of which can be seen in [3].

REFERENCES

[1] CLF based MIQP + Impedance Control on AMBER. `http://youtu.be/5TuTyKhMNiU`.

[2] Learning Impedance Controller Parameters for Lower-Limb Prostheses. `http://youtu.be/AzF5-gqtRbc`.

[3] Sustainable Walking of AMBER2. `http://youtu.be/d6oM5sLI9vA`.

[4] Video of Simulation Results. `http://youtu.be/Z0oWlYwgD-A`.

[5] Navid Aghasadeghi, Huihua Zhao, Levi J Hargrove, Aaron D Ames, Eric J Perreault, and Timothy Bretl. Learning impedance controller parameters for lower-limb prostheses. *IEEE: IROS*, 2013.

[6] A. D. Ames. First steps toward automatically generating bipedal robotic walking from human data. In *8th International Workshop on Robotic Motion and Control, RoMoCo'11*, Bukowy Dworek, 2011.

[7] Aaron D Ames. Human-inspired control of bipedal robots via control lyapunov functions and quadratic programs. In *Proceedings of the 16th international conference on Hybrid systems: computation and control*, pages 31–32. ACM, 2013.

[8] A.D. Ames, K. Galloway, and J.W. Grizzle. Control lyapunov functions and hybrid zero dynamics. In *Decision and Control (CDC), 2012 IEEE 51st Annual Conference on*, pages 6837–6842, 2012.

[9] D.P. Atherton and S. Majhi. Limitations of pid controllers. In *American Control Conference*, pages 3843–3847, 1999.

[10] Christopher G Atkeson and Stefan Schaal. Robot learning from demonstration. In *ICML*, volume 97, pages 12–20, 1997.

[11] Samuel Au, Max Berniker, and Hugh Herr. Powered ankle-foot prosthesis to assist level-ground and stair-descent gaits. *Neural Networks*, 21(4):654 – 666, 2008.

[12] A. Blank, A.M. Okamura, and L.L. Whitcomb. User comprehension of task performance with varying impedance in a virtual prosthetic arm: A pilot study. In *Biomedical Robotics and Biomechatronics (BioRob), 2012 4th IEEE RAS EMBS International Conference*, pages 500–507.

[13] J.A. Blaya and H. Herr. Adaptive control of a variable-impedance ankle-foot orthosis to assist drop-foot gait. *Neural Systems and Rehabilitation Engineering, IEEE Transactions on*, 12(1):24–31, 2004.

[14] A.W. Boehler, K.W. Hollander, T.G. Sugar, and Dosun Shin. Design, implementation and test results of a robust control method for a powered ankle foot orthosis (afo). In *Robotics and Automation, ICRA, IEEE*, pages 2025–2030, 2008.

[15] Neville Hogan. Impedance control: An approach to manipulation. pages 304–313, 1984.

[16] K.W. Hollander and T.G. Sugar. A robust control concept for robotic ankle gait assistance. In *Rehabilitation Robotics, ICORR, IEEE 10th International Conference on*, pages 119–123, 2007.

[17] Y. Hürmüzlü and D. B. Marghitu. Rigid body collions of planar kinematic chains with multiple contact points. *Intl. J. of Robotics Research*, 13(1):82–92, February 1994.

[18] René Jimenez-Fabian and Olivier Verlinden. Review of control algorithms for robotic ankle systems in lower-limb orthoses, prostheses, and exoskeletons. *Medical engineering & physics*, 34(4):397–408.

[19] Jun Nakanishi, Jun Morimoto, Gen Endo, Gordon Cheng, Stefan Schaal, and Mitsuo Kawato. Learning from demonstration and adaptation of biped locomotion. *Robotics and Autonomous Systems*, 47(2):79–91, 2004.

[20] T.S. Parker and L.O. Chua. Practical numerical algorithms for chaotic systems. 1989.

[21] Dejan Popovic, Rajko Tomovic, Dejan Tepavac, and Laszlo Schwirtlich. Control aspects of active above-knee prosthesis. *International Journal of Man-Machine Studies*, 35(6):751 – 767, 1991.

[22] Matthew J Powell, Huihua Zhao, and Aaron D Ames. Motion primitives for human-inspired bipedal robotic locomotion: walking and stair climbing. In *Robotics and Automation (ICRA), IEEE International Conference*, pages 543–549, 2012.

[23] S. S. Sastry. *Nonlinear Systems: Analysis, Stability and Control*. Springer, New York, June 1999.

[24] Frank Sup, Amit Bohara, and Michael Goldfarb. Design and Control of a Powered Transfemoral Prosthesis. *The International journal of robotics research*, 27(2):263–273, February 2008.

[25] Toshio Tsuji, Keisuke Shima, Nan Bu, and Osamu Fukuda. Biomimetic impedance control of an emg-based robotic hand.

[26] Radcliffe C. W. Biomechanical basis for the design of prosthetic knee mechanisms. *Rehabilitation Engineering International Seminar*, 1980.